SUPPLEMENTARY TABLE AND FIGURES

	ClpX subunit							
	A	B	C	D	E	F	substrate	ClpX
DHFR	ATP	ATP	ATP	ADP	ADP	ADP	DHFR-ssrA	ΔN
8ET3	ATPγS	ATPγS	ATPγS	ATPγS	ADP	ADP	SspB/GFP-ssrA	full-length
6WRF	ATPγS	ATPγS	ATPγS	ATPγS	ATPγS	ADP	GFP-ssrA	ΔN
6WSG	apo	ATPγS	ATPγS	ATPγS	ATPγS	ATPγS	GFP-ssrA	ΔN
6VFS	ADP	ATP	ATP	ATP	ATP	ADP	GFP-ssrA	ΔN
6VFX	ATP	ATP	ATP	ATP	ATP	ADP	GFP-ssrA	ΔN
6PP5	ATPγS	ATPγS	ATPγS	ATPγS	ATPgS	ADP	unknown	ΔN
6PP6	ATPγS	ATPγS	ATPγS	ATPγS	ATPγS	ADP	unknown	ΔN
6PP7	ADP	ATPγS	ATPγS	ATPγS	ATPγS	ATPγS	unknown	ΔN
6PP8	ATPγS	ATPγS	ATPγS	ATPγS	ATPγS	ADP	unknown	ΔN
8E91	ATPγS	ATPγS	ATPγS	ATPγS	ADP	ADP	none	full-length
8E8Q	ATP	ATP	ATP	ATP	ADP	ADP	none	ΔN
8E7V	ATP	ATP	ATP	ATP	ADP	ADP	none	ΔN

Table S1. Nucleotide occupancy. Nucleotide occupancy of subunits in different ClpX cryo-EM structures (Fei, Bell *et al.* 2020, Fei, Bell *et al.* 2020, Ripstein, Vahidi *et al.* 2020, Ghanbarpour, Cohen *et al.* 2023, Ghanbarpour, Fei *et al.* 2023). Red designates subunits that appear catalytically active for ATP hydrolysis. Blue designates subunits that are catalytically inactive either because they contain ADP, or because they contain ATP/ATPγS but the side chain of the Arg^{307}-finger residue, which is required for ATP hydrolysis, is disengaged.

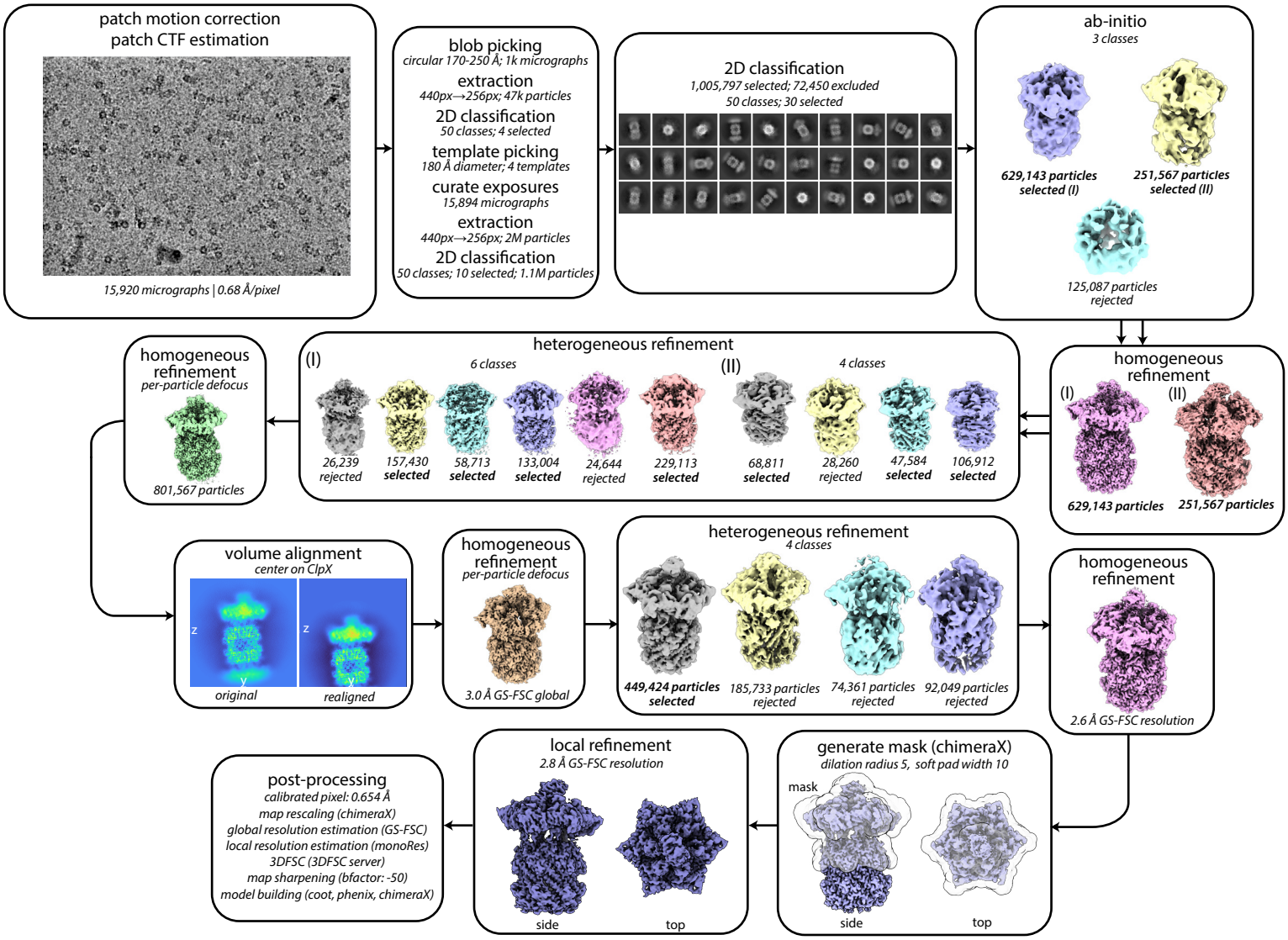

Figure S1. Image processing workflow. CryoSPARC processing workflow for single-chain ClpX^{ΔN}/ClpP/DHFR•MTX particles. Job names, job details, and non-default parameters (italicized) are noted in each box.

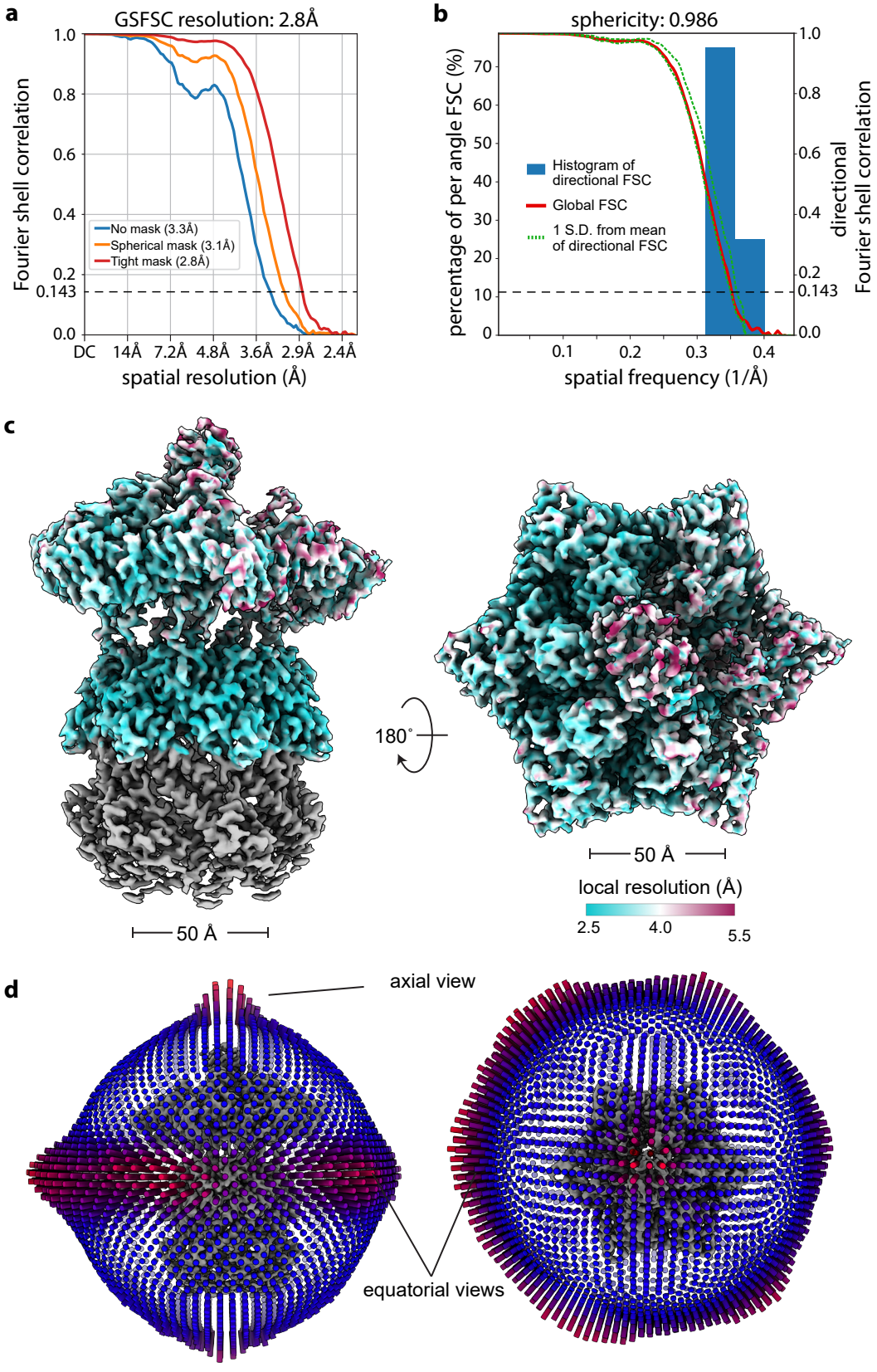

Figure S2. Estimates of GSFSC resolution. **(a)** Global resolution estimated by the gold-standard Fourier Shell Correlation method as implemented in CryoSPARC (Punjani, Rubinstein *et al*. 2017). **(b)** Directional FSC as estimated by the 3DFSC server (Tan, Baldwin *et al.* 2017). **(c)** Density map colored by local resolution as estimated by cryoSPARC's implementation of monoRes (Vilas, Gomez-Blanco *et al.* 2018). Regions outside of the local refinement mask colored grey. **(d)** Projection-angle distribution.

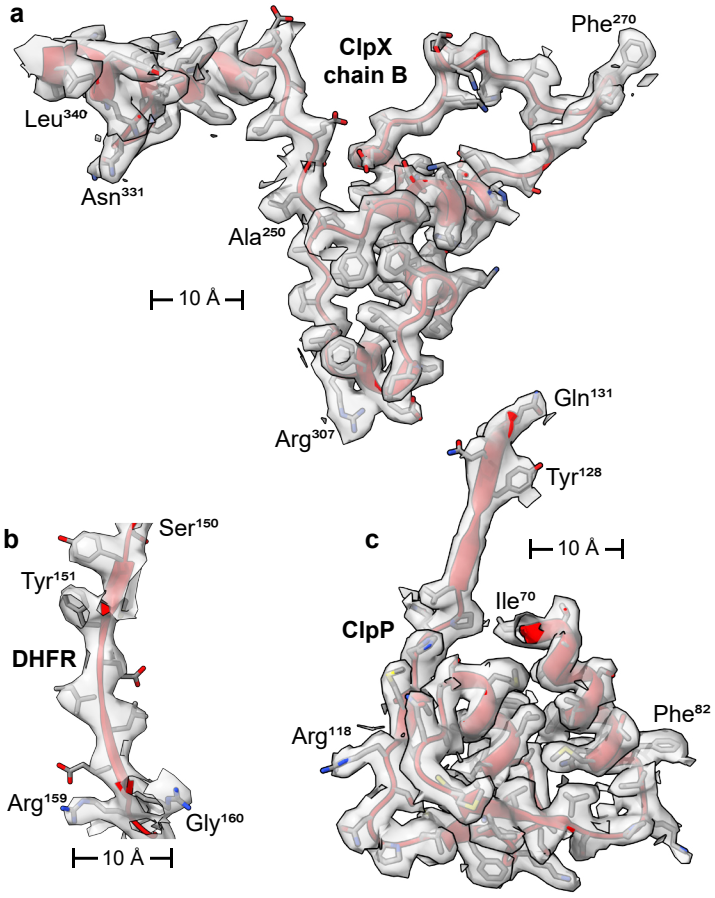

Figure S3. Cryo-EM density map and atomic model. Cryo-EM density map (grey semitransparent surface) overlayed on the fitted atomic models, with secondary structure elements colored red, and sidechains colored by atom type. **(a)** ClpX residues 270-340 of chain B. **(b)** DHFR residues 150-160. **(c)** ClpP residues 131-170 of chain i.

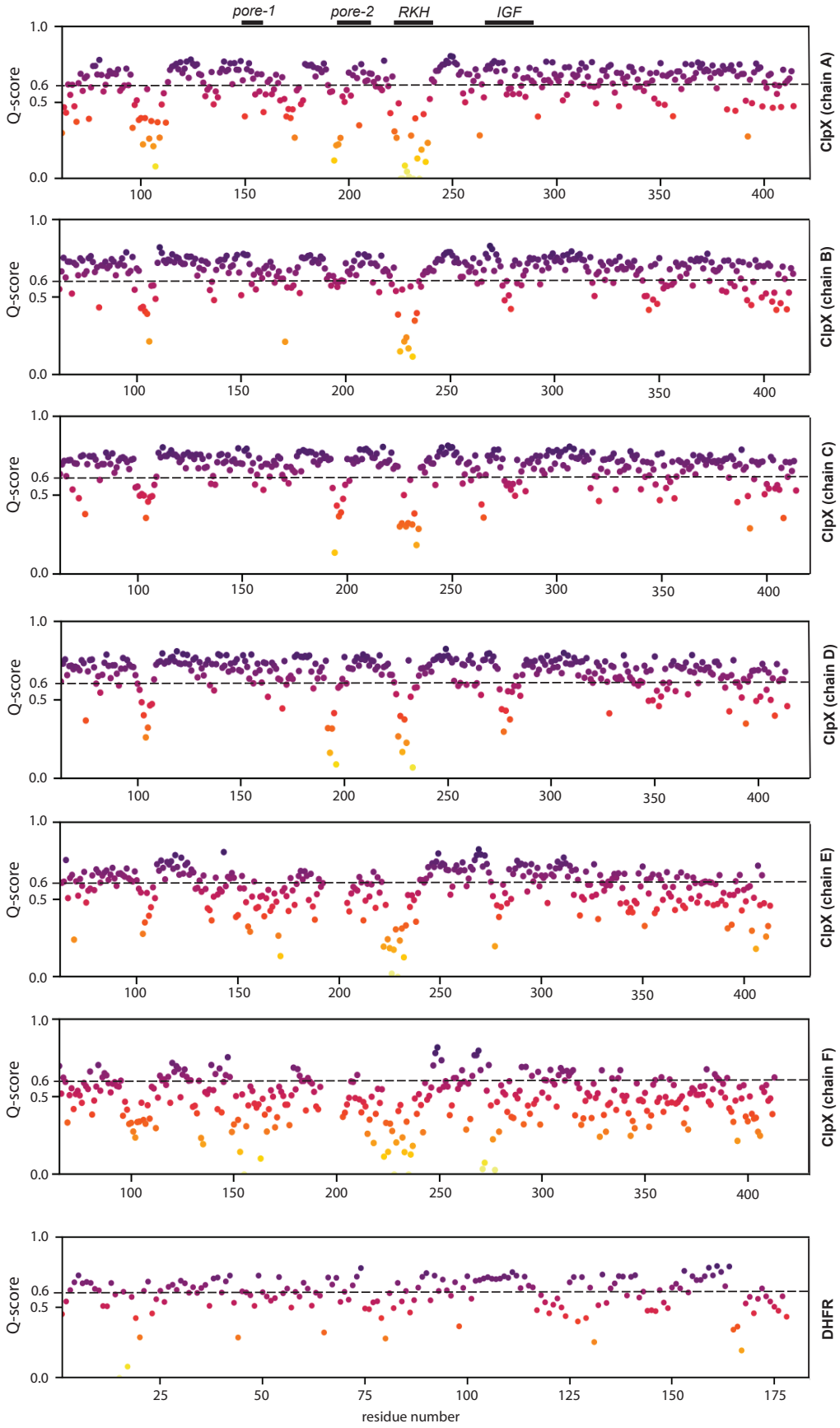

Figure S4. Map-model assessment. Calculated Q-scores (Pintilie, Zhang *et al.* 2020) for ClpX subunits and DHFR. Expected Q-score (0.6) given map resolution noted, and location of ClpX flexible loops annotated.

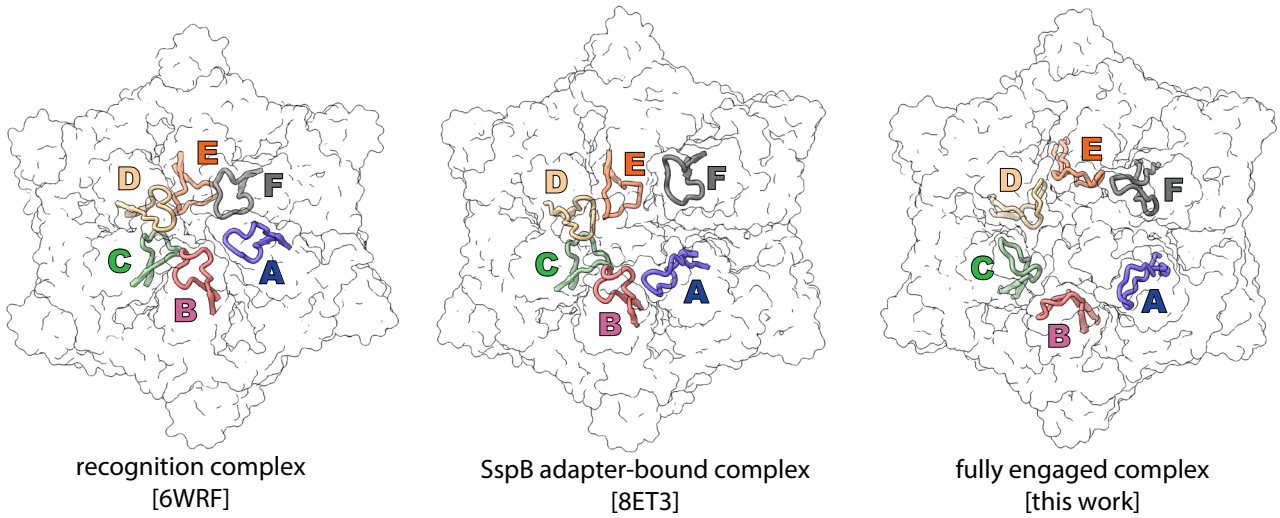

Figure S5. Conformational flexibility of the ClpX RKH loops. Diverse conformations of RKH loops (residues 218-240) from ClpXP structures 6WRF (left) (Fei, Bell *et al.* 2020), 8ET3 (center) (Ghanbarpour, Fei *et al.* 2023), and the DHFR-bound structure presented in this paper (right). Subunit colors: A (purple), B (salmon), C (green); D (wheat), E (orange), and F (gray).

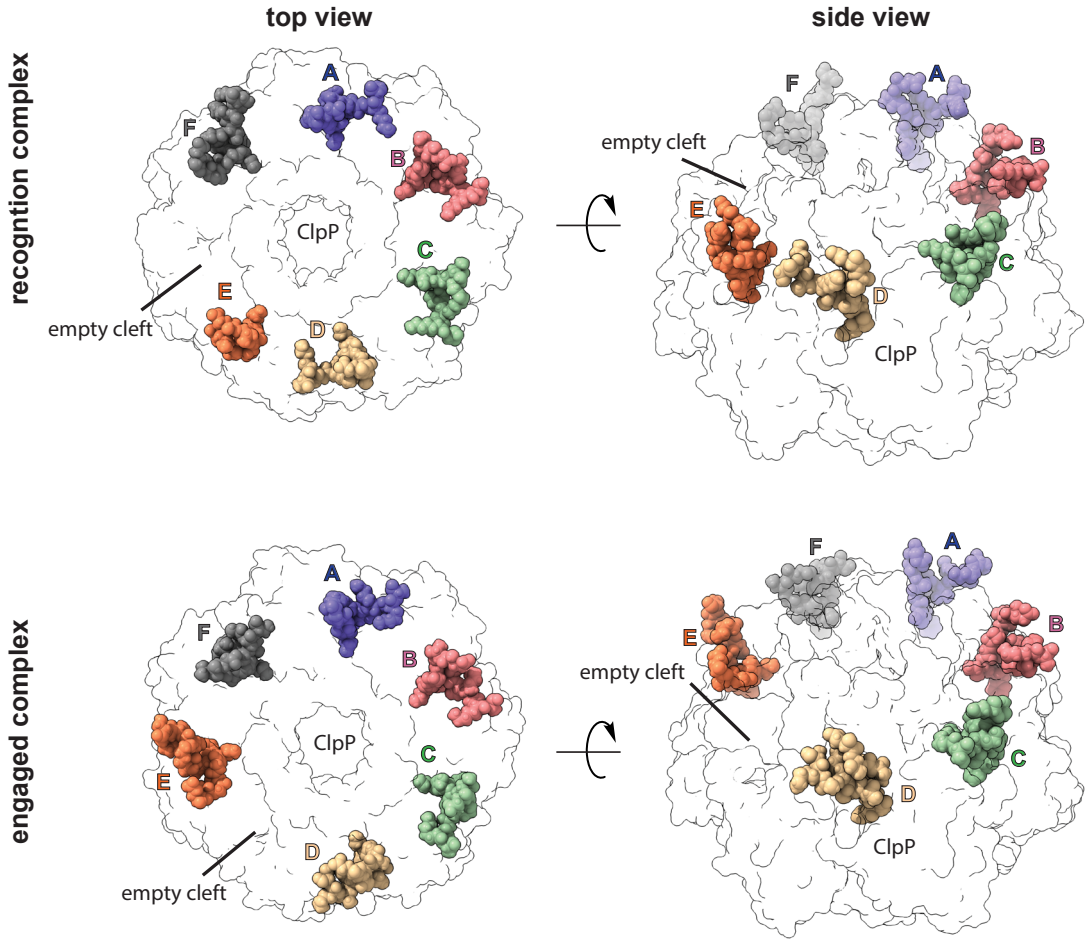

Figure S6. Rearrangement of ClpX-ClpP contacts. In a complex of ClpX bound to an ssrA degron (pdb 6WRF), the empty binding cleft on a ClpP heptamer is between the IGF loops of ClpX subunits E and F (top row). This arrangement is observed in most ClpXP structures (Fei, Bell *et al.* 2020, Fei, Bell *et al.* 2020, Ripstein, Vahidi *et al.* 2020, Ghanbarpour, Cohen *et al.* 2023). In the DHFR-engaged ClpXP structure (bottom row), the IGF loop of chain E moves into a binding cleft on the surface of the ClpP heptamer that is unoccupied in ClpXP structures except 8ET3 (Ghanbarpour, Fei *et al.* 2023). These loop docking interactions are depicted from top (left column), or side (right column) views.

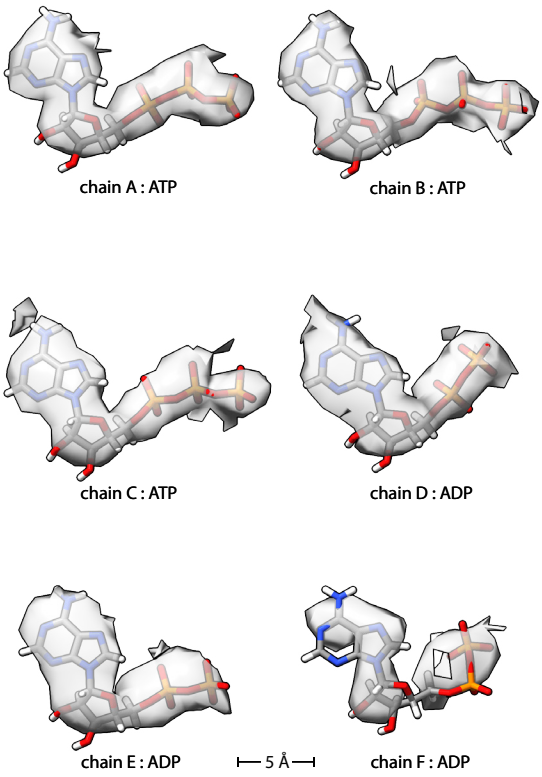

Figure S7. Density for ATP or ADP bound to different ClpX subunits in the DHFR-bound structure. Density map (grey semi-transparent surface) is overlayed on atomic models, which are colored by atom type.

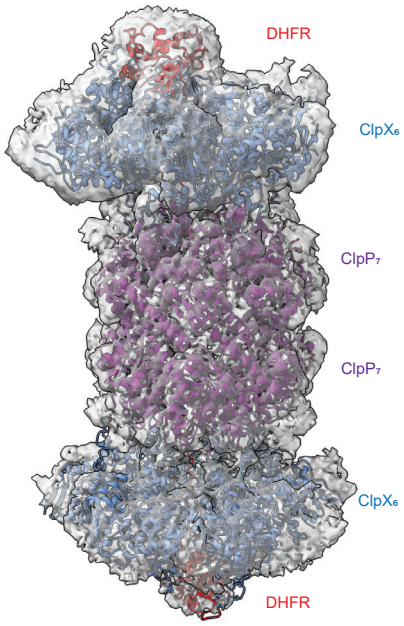

Figure S8. Low-resolution structure of a second ClpX•DHFR complex bound to the bottom heptameric ring of $ClpP_{14}$. The distal ClpX•DHFR complex adopts multiple registers in relation to the top complex and has lower resolution as a consequence of conformational averaging.